REPORT DOCUMENTATION PAGE

Form Approved OMB NO. 0704-0188

1. REPORT DATE (DD-MM-YYYY)	2. REPORT TYPE	3. DATES COVERED (From - To)
27-08-2016	Final Report	15-Sep-2014 - 14-Sep-2017

4. TITLE AND SUBTITLE
Final Report: Nanostructured High Entropy Alloys

5a. CONTRACT NUMBER
W911NF-14-1-0627

5b. GRANT NUMBER

5c. PROGRAM ELEMENT NUMBER
611102

6. AUTHORS
Enrique Lavernia

5d. PROJECT NUMBER

5e. TASK NUMBER

5f. WORK UNIT NUMBER

7. PERFORMING ORGANIZATION NAMES AND ADDRESSES
University of California - Davis
Sponsored Programs
1850 Research Park Drive, Suite 300
Davis, CA 95618 -6153

8. PERFORMING ORGANIZATION REPORT NUMBER

9. SPONSORING/MONITORING AGENCY NAME(S) AND ADDRESS (ES)
U.S. Army Research Office
P.O. Box 12211
Research Triangle Park, NC 27709-2211

10. SPONSOR/MONITOR'S ACRONYM(S)
ARO

11. SPONSOR/MONITOR'S REPORT NUMBER(S)
65347-MS.7

12. DISTRIBUTION AVAILIBILITY STATEMENT
Approved for Public Release; Distribution Unlimited

13. SUPPLEMENTARY NOTES
The views, opinions and/or findings contained in this report are those of the author(s) and should not contrued as an official Department of the Army position, policy or decision, unless so designated by other documentation.

14. ABSTRACT
The objective of this research program was to establish a fundamental framework that can be used to advance our knowledge of nanostructured high entropy alloy (HEA) materials and their processing, microstructure and performance. This program was conducted via a synergistic approach involving materials synthesis and processing, microstructural and mechanical behavior studies. Through the performance period (September 10, 2014 – July 31, 2016), the following studies were conducted: (1) A medium entropy alloy AlCoNiFe was selected for systematic studies of Ti additions and the influence of materials processing/synthesis on microstructural evolution and

15. SUBJECT TERMS
High entropy alloys, severe plastic deformation, nanostructure, mechanical behavior

16. SECURITY CLASSIFICATION OF:			17. LIMITATION OF ABSTRACT	15. NUMBER OF PAGES	19a. NAME OF RESPONSIBLE PERSON
a. REPORT	b. ABSTRACT	c. THIS PAGE			Enrique Lavernia
UU	UU	UU	UU		19b. TELEPHONE NUMBER 949-824-6296

Report Title

Final Report: Nanostructured High Entropy Alloys

ABSTRACT

The objective of this research program was to establish a fundamental framework that can be used to advance our knowledge of nanostructured high entropy alloy (HEA) materials and their processing, microstructure and performance. This program was conducted via a synergistic approach involving materials synthesis and processing, microstructural and mechanical behavior studies. Through the performance period (September 10, 2014 – July 31, 2016), the following studies were conducted: (1) A medium entropy alloy AlCoNiFe was selected for systematic studies of Ti additions and the influence of materials processing/synthesis on microstructural evolution and mechanical behavior. (2) An AlNiFeCrCo HEA was investigated to understand the influence of Co and materials processing/synthesis techniques on microstructural evolution and mechanical behavior. (3) An equiatomic CoNiFeAlTi HEA was synthesized and the effect of high atomic concentration of Ti and Al on the microstructure, phase transformations and mechanical behavior was studied. (4) Phase transformations, microstructure and strengthening mechanisms in a near-equiatomic CoNiFeAlCu HEA were investigated. (5) The influence of Cr on alloying behavior, microstructure and mechanical behavior of an AlTiCoNiFeCr HEA was studied. (6) Fabrication of ingot AlCoCrCuFeNi HEA was carried out. (7) High pressure torsion processing of AlCoCrCuFeNi HEA was applied to investigate the effects of grain refinement on mechanical behavior of HEAs. (8) Synthesis and processing of nanocrystalline AlCoCrCuFeNi HEA via gas atomization, cryomilling and spark plasma sintering (SPS) was explored. (9) Investigation of microstructure and mechanical behavior of a precipitation-hardened Fe27Ni27Co26Cu10Ti10 HEA. (10) Thermal stability and mechanical behavior of a single phased Fe27Ni27Co26Cu10Mn10 HEA.
Key research activities conducted during the performance period of 08/01/2015-07/31/2016 are summarized in this final report. Please refer to 2014-2015 interim report (09/10/2014 – 07/31/2015) for previously reported results and accomplishments in association with the above (1) – (4).

Enter List of papers submitted or published that acknowledge ARO support from the start of the project to the date of this printing. List the papers, including journal references, in the following categories:

(a) Papers published in peer-reviewed journals (N/A for none)

Received		Paper
08/18/2016	4	Zhiqiang Fu, Weiping Chen, Haiming Wen, Dalong Zhang, Zhen Chen, Baolong Zheng, Yizhang Zhou, Enrique J. Lavernia. Microstructure and strengthening mechanisms in an FCC structured single-phase nanocrystalline Co25Ni25Fe25Al7.5Cu17.5 high-entropy alloy, Acta Materialia , (07 2015): 59. doi:
08/24/2016	6	3) Zhiqiang Fu, Weiping Chen, Haiming Wen, Sam Morgan, Fei Chen, Baolong Zheng, Yizhang Zhou, Lianmeng Zhang, Enrique J. Lavernia. Microstructure and mechanical behavior of a novel Co20Ni20Fe20Al20Ti20 alloy fabricated by mechanical alloying and spark plasma sintering, materials Science and Engineering A, ( ): 10. doi:
08/28/2015	1	Haiming Wen, Enrique J. Lavernia, Zhiqiang Fu, Weiping Chen, Zhen Chen. Influence of Ti addition and sintering method on microstructure and mechanical behavior of a medium-entropy AlCoNiFe alloy, Materials Science and Engineering A, (12 2014): 137. doi:
08/28/2015	2	Weiping Chen, Haiming Wen, Zhen Chen, Enrique J. Laverniab, Zhiqiang Fu. Effects of Co and sintering method on microstructure and mechanical behavior of a high-entropy Al0.6NiFeCrCo alloy prepared by powder metallurgy, Journal of Alloys and Compounds, (06 2015): 175. doi:
TOTAL:	**4**	

Number of Papers published in peer-reviewed journals:

(b) Papers published in non-peer-reviewed journals (N/A for none)

Received Paper

TOTAL:

Number of Papers published in non peer-reviewed journals:

(c) Presentations

1) Zhiqiang Fu, Weiping Chen, Haiming Wen, Dalong Zhang, Zhen Chen, Baolong Zheng, Enrique J. Lavernia, Design and mechanical behavior of nanocrystalline Co25Ni25Fe25Al7.5Cu17.5 high-entropy alloy with ultra-high strength, presentation, MS&T2015, October 5-7, Columbus, Ohio.
2) Zhiqiang Fu, Weiping Chen, Baolong Zheng, Yaojun Lin, Fei Chen, Lianmeng Zhang, Yizhang Zhou, Enrique J. Lavernia. Influence of Cr removal on alloying behavior, microstructure and mechanical behavior of ultra-fine grained Al0.8Ti0.2CoNiFeCr high entropy alloy, presentation, 2016 TMS Annual Meeting, February 14-18, Nashville, Tennessee.
3) Baolong Zheng, Zhiqiang Fu, Yaojun Lin, Lilia Kurmanaeva, Julia Ivanisenko, Yizhang Zhou, Fei Chen, Horst Hahn, Lianmeng Zhang, and Enrique J. Lavernia, Microstructure evolution, phase stability and mechanical behavior of ultra-fine grained AlFeNiCuCoCr high entropy alloy processed by severe plastic deformation, presentation, 2016 TMS Annual Meeting, February 14-18, Nashville, Tennessee.

Number of Presentations: 3.00

Non Peer-Reviewed Conference Proceeding publications (other than abstracts):

Received Paper

TOTAL:

Number of Non Peer-Reviewed Conference Proceeding publications (other than abstracts):

Peer-Reviewed Conference Proceeding publications (other than abstracts):

Received Paper

TOTAL:

Number of Peer-Reviewed Conference Proceeding publications (other than abstracts):

(d) Manuscripts

Received Paper

TOTAL:

Number of Manuscripts:

Books

Received Book

TOTAL:

Received Book Chapter

TOTAL:

Patents Submitted

Patents Awarded

Awards

Alexander von Humboldt Foundation Research Award, 2016; Leadership Award, TMS Society, Warrendale, PA, 2016; Hispanic Hall of Fame, HEENAC Great Minds in STEM, 2015

Graduate Students

NAME	PERCENT_SUPPORTED	Discipline
Benjamin MacDonald	0.49	
Zhiqiang Fu	0.00	
FTE Equivalent:	**0.49**	
Total Number:	**2**	

Names of Post Doctorates

NAME	PERCENT_SUPPORTED
Zhiqiang Fu	1.00
Kaka Ma	0.20
FTE Equivalent:	**1.20**
Total Number:	**2**

Names of Faculty Supported

NAME	PERCENT_SUPPORTED	National Academy Member
Enrique Lavernia	0.02	Yes
FTE Equivalent:	**0.02**	
Total Number:	**1**	

Names of Under Graduate students supported

NAME	PERCENT_SUPPORTED
FTE Equivalent:	
Total Number:	

Student Metrics

This section only applies to graduating undergraduates supported by this agreement in this reporting period

The number of undergraduates funded by this agreement who graduated during this period: 0.00

The number of undergraduates funded by this agreement who graduated during this period with a degree in science, mathematics, engineering, or technology fields:..... 0.00

The number of undergraduates funded by your agreement who graduated during this period and will continue to pursue a graduate or Ph.D. degree in science, mathematics, engineering, or technology fields:..... 0.00

Number of graduating undergraduates who achieved a 3.5 GPA to 4.0 (4.0 max scale):..... 0.00

Number of graduating undergraduates funded by a DoD funded Center of Excellence grant for Education, Research and Engineering:..... 0.00

The number of undergraduates funded by your agreement who graduated during this period and intend to work for the Department of Defense 0.00

The number of undergraduates funded by your agreement who graduated during this period and will receive scholarships or fellowships for further studies in science, mathematics, engineering or technology fields:..... 0.00

Names of Personnel receiving masters degrees

NAME
Total Number:

Names of personnel receiving PHDs

NAME
Zhiqiang Fu
Total Number: **1**

Names of other research staff

NAME	PERCENT_SUPPORTED
Baolong Zheng	0.10
FTE Equivalent:	**0.10**
Total Number:	**1**

Sub Contractors (DD882)

Inventions (DD882)

Scientific Progress

See Attachment

Technology Transfer

Our team has been interacting with national laboratories and private sectors to explore potential applications of novel high entropy alloys.

REPORT DOCUMENTATION PAGE

Form Approved
OMB NO. 0704-0188

1. AGENCY USE ONLY (Leave Blank)	2. REPORT DATE 08/25/2016	3. REPORT TYPE AND DATES COVERED Final Technical Report September 10, 2014 – July 31, 2016

4. TITLE AND SUBTITLE

Nanostructured High Entropy Alloys

5. FUNDING NUMBERS

ARO W911NF 14-1-0627

6. AUTHOR(S)
Enrique J. Lavernia

7. PERFORMING ORGANIZATION NAME(S) AND ADDRESS(ES)
University of California, Davis
One shields Ave
Davis, CA 95616

8. PERFORMING ORGANIZATION REPORT NUMBER

9. SPONSORING / MONITORING AGENCY NAME(S) AND ADDRESS(ES)
U. S. Army Research Office
P.O. Box 12211
Research Triangle Park, NC 27709-2211

10. SPONSORING / MONITORING AGENCY REPORT NUMBER

11. SUPPLEMENTARY NOTES

The views, opinions and/or findings contained in this report are those of the author(s) and should not be construed as an official Department of the Army position, policy or decision, unless so designated by other documentation.

12 a. DISTRIBUTION / AVAILABILITY STATEMENT

Approved for public release; distribution unlimited.

12 b. DISTRIBUTION CODE

13. ABSTRACT (Maximum 200 words)

The objective of this research program was to establish a fundamental framework that can be used to advance our knowledge of nanostructured high entropy alloy (HEA) materials and their processing, microstructure and performance. This program was conducted via a synergistic approach involving materials synthesis and processing, microstructural and mechanical behavior studies. Through the performance period (September 10, 2014 – July 31, 2016), the following studies were conducted: (1) A medium entropy alloy AlCoNiFe was selected for systematic studies of Ti additions and the influence of materials processing/synthesis on microstructural evolution and mechanical behavior. (2) An AlNiFeCrCo HEA was investigated to understand the influence of Co and materials processing/synthesis techniques on microstructural evolution and mechanical behavior. (3) An equiatomic CoNiFeAlTi HEA was synthesized and the effect of high atomic concentration of Ti and Al on the microstructure, phase transformations and mechanical behavior was studied. (4) Phase transformations, microstructure and strengthening mechanisms in a near-equiatomic CoNiFeAlCu HEA were investigated. (5) The influence of Cr on alloying behavior, microstructure and mechanical behavior of an AlTiCoNiFeCr HEA was studied. (6) Fabrication of ingot AlCoCrCuFeNi HEA was carried out. (7) High pressure torsion processing of AlCoCrCuFeNi HEA was applied to investigate the effects of grain refinement on mechanical behavior of HEAs. (8) Synthesis and processing of nanocrystalline AlCoCrCuFeNi HEA via gas atomization, cryomilling and spark plasma sintering (SPS) was explored. (9) Investigation of microstructure and mechanical behavior of a precipitation-hardened $Fe_{27}Ni_{27}Co_{26}Cu_{10}Ti_{10}$ HEA. (10) Thermal stability and mechanical behavior of a single phased $Fe_{27}Ni_{27}Co_{26}Cu_{10}Mn_{10}$ HEA.

Key research activities conducted during the performance period of 08/01/2015-07/31/2016 are summarized in this final report. Please refer to 2014-2015 interim report (09/10/2014 – 07/31/2015) for previously reported results and accomplishments in association with the above (1) – (4).

14. SUBJECT TERMS

High entropy alloys, severe plastic deformation, nanostructure, mechanical behavior

15. NUMBER OF PAGES

16. PRICE CODE

17. SECURITY CLASSIFICATION OR REPORT	18. SECURITY CLASSIFICATION ON THIS PAGE	19. SECURITY CLASSIFICATION OF ABSTRACT	20. LIMITATION OF ABSTRACT
UNCLASSIFIED	**UNCLASSIFIED**	**UNCLASSIFIED**	**UL**

REPORT DOCUMENTATION PAGE (SF298)
(Continuation Sheet)

1. List of Publications and Presentations

1) Zhiqiang Fu, Weiping Chen, Zhen Chen, Haiming Wen, Enrique J. Lavernia, Influence of Ti addition and sintering method on microstructure and mechanical behavior of a medium-entropy $Al_{0.6}CoNiFe$ alloy, Materials Science & Engineering A, 619, pp. 137–145, 2014.
2) Zhiqiang Fu, Weiping Chen, Haiming Wen, Zhen Chen, Enrique J. Lavernia, Effects of Co and sintering method on microstructure and mechanical behavior of a high-entropy $Al_{0.6}NiFeCrCo$ alloy prepared by powder metallurgy, Journal of Alloys and Compounds, 646, pp. 175–182, 2015.
3) Zhiqiang Fu, Weiping Chen, Haiming Wen, Sam Morgan, Fei Chen, Baolong Zheng, Yizhang Zhou, Lianmeng Zhang, Enrique J. Lavernia, Microstructure and mechanical behavior of a novel $Co_{20}Ni_{20}Fe_{20}Al_{20}Ti_{20}$ alloy fabricated by mechanical alloying and spark plasma sintering, Materials Science & Engineering A, 644, pp. 10–16, 2015.
4) Zhiqiang Fu, Weiping Chen, Haiming Wen, Dalong Zhang, Zhen Chen, Baolong Zheng, Yizhang Zhou, Enrique J. Lavernia, Microstructure and strengthening mechanisms in an FCC structured single-phase nanocrystalline $Co_{25}Ni_{25}Fe_{25}Al_{7.5}Cu_{17.5}$ high-entropy alloy, Acta Materialia, 107, pp. 59–71, 2016.
5) Zhiqiang Fu, Weiping Chen, Haiming Wen, Dalong Zhang, Zhen Chen, Baolong Zheng, Enrique J. Lavernia, Design and mechanical behavior of nanocrystalline $Co_{25}Ni_{25}Fe_{25}Al_{7.5}Cu_{17.5}$ high-entropy alloy with ultra-high strength, presentation, MS&T2015, October 5-7, Columbus, Ohio.
6) Zhiqiang Fu, Weiping Chen, Baolong Zheng, Yaojun Lin, Fei Chen, Lianmeng Zhang, Yizhang Zhou, Enrique J. Lavernia. Influence of Cr removal on alloying behavior, microstructure and mechanical behavior of ultra-fine grained $Al_{0.8}Ti_{0.2}CoNiFeCr$ high entropy alloy, presentation, 2016 TMS Annual Meeting, February 14-18, Nashville, Tennessee.
7) Baolong Zheng, Zhiqiang Fu, Yaojun Lin, Lilia Kurmanaeva, Julia Ivanisenko, Yizhang Zhou, Fei Chen, Horst Hahn, Lianmeng Zhang, and Enrique J. Lavernia, Microstructure evolution, phase stability and mechanical behavior of ultra-fine grained AlFeNiCuCoCr high entropy alloy processed by severe plastic deformation, presentation, 2016 TMS Annual Meeting, February 14-18, Nashville, Tennessee.

2. Scientific Personnel

Zhiqiang Fu, Graduate Student / Post-doctoral Researcher
Benjamin MacDonald, Graduate Student
Kaka Ma, Post-doctoral Researcher
Dr. Baolong Zheng, Assistant Project Scientist

3. Scientific Progress and Accomplishments

Key research activities conducted during the performance period of 08/01/2015-07/31/2016 are summarized in this final report.

3.1 Investigation of alloying, microstructure and mechanical behavior of an AlTiCoNiFeCr HEA

In this work, we studied the influence of Cr removal on the alloying behavior, microstructure and mechanical behavior of an ultra-fine grained (UFG) $Al_{0.8}Ti_{0.2}CoNiFeCr$ HEA. This HEA materials was produced by first, mechanically alloying (MA) of powders from constituent elemental powders, followed by consolidation via spark plasma sintering (SPS) technique. The MA'ed $Al_{0.8}Ti_{0.2}CoNiFeCr$ powders comprise mostly a BCC phase (~85 vol.%) with a small amount of FCC phase (~15 vol.%), whereas the MA'ed $Al_{0.8}Ti_{0.2}CoNiFe$ powders present similar phases to those in the MA'ed $Al_{0.8}Ti_{0.2}CoNiFeCr$ powders. Interestingly, the SPS processed UFG $Al_{0.8}Ti_{0.2}CoNiFeCr$ alloy contains mostly an FCC phase (~78 vol.%) and some BCC phase (~22 vol.%); in contrast, the SPS-processed UFG $Al_{0.8}Ti_{0.2}CoNiFe$ alloy consists of a more rich BCC phase (~53 vol.%) and an FCC phase (~47 vol.%). In addition, the SPS-processed $Al_{0.8}Ti_{0.2}CoNiFe$ alloy exhibits

slightly higher yield strength, compressive strength and hardness but lower ductility than those of the SPS processed $Al_{0.8}Ti_{0.2}CoNiFeCr$ alloy.

Influence of Cr removal on alloying behavior: Figure 3.1.1(a) shows the XRD patterns of the $Al_{0.8}Ti_{0.2}CoNiFeCr$ HEA powders with different milling time. The anticipated alloying sequence is: Al→Co→Ni→Fe→Ti →Cr, due to the fact that alloying rates of constituent elements with the same concentrations are inversely proportional to their melting points. After 6 h of milling, Al essentially disappears. As milling time increases to 15 h, Co disappears. After 30 h of milling, most constituent elements disappear, and a primary BCC solid-solution phase (~85 vol.%) with a small amount of FCC solid-solution phase (~15 vol.%) are formed; As milling time further increases to 45 h and 49 h, there is no significant phase evolution except evident peak broadening (grain refinement). Figure 3.1.1(b) shows the XRD patterns of the $Al_{0.8}Ti_{0.2}CoNiFe$ HEA powders with different milling time. Similar to that in $Al_{0.8}Ti_{0.2}CoNiFeCr$ system, the anticipated alloying sequence is: Al→Co→Ni→Fe→Ti. After 6 h of milling, Al essentially disappears. As milling time increases to 15 h, both Co and Ni disappears, however, Ni still exists in the MA'ed $Al_{0.8}Ti_{0.2}CoNiFeCr$ powders. After 30 h of milling, all of the elements disappear, the $Al_{0.8}Ti_{0.2}CoNiFe$ powders present similar phases to those in the MA'ed $Al_{0.8}Ti_{0.2}CoNiFeCr$ powders. Similarly, as milling time increases (30 h-49 h), there is no significant phase evolution except evident peak broadening.

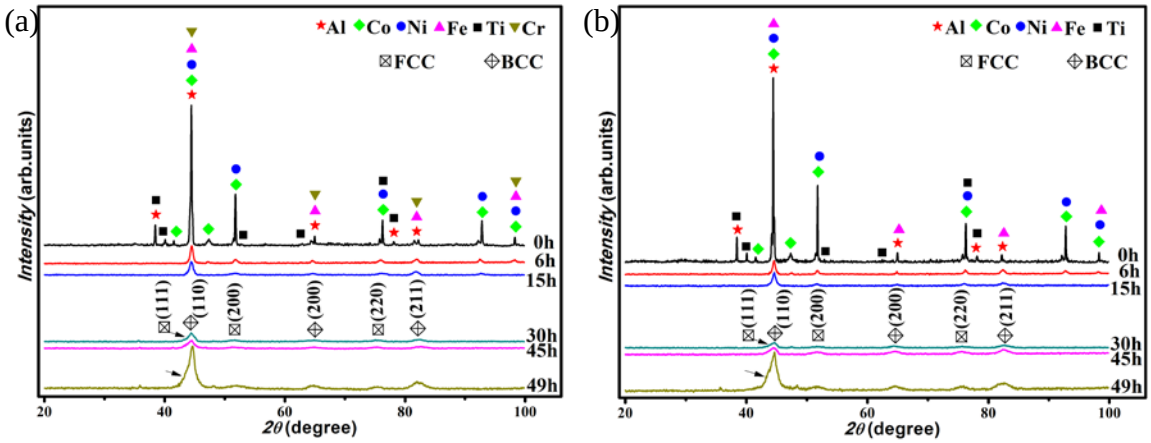

Fig. 3.1.1: XRD patterns of powders with different milling time. (a) $Al_{0.8}Ti_{0.2}CoNiFeCr$, (b) $Al_{0.8}Ti_{0.2}CoNiFe$.

Influence of Cr removal on microstructure: Figure 3.1.2 shows the XRD patterns of bulk ($Al_{0.8}Ti_{0.2}CoNiFeCr$ and $Al_{0.8}Ti_{0.2}CoNiFe$) HEAs after SPS. Bulk $Al_{0.8}Ti_{0.2}CoNiFeCr$ HEA contains mostly an FCC phase (~78 vol.%) and some BCC phase (~22 vol.%). With removal of Cr, bulk $Al_{0.8}Ti_{0.2}CoNiFe$ HEA consists of a more rich BCC phase (~53 vol.%) and an FCC phase (~47 vol.%). For these two HEAs, the primary phases of the MA'ed powders are BCC phase, indicating phase transformation took place during SPS. Because of the solubility extension generated during the non-equilibrium MA process, supersaturated solid-solutions are formed in the milled powders, which consist of a primary BCC phase and an FCC phase. These metastable supersaturated solid-solution phases transform to equilibrium phases during sintering or heating, leading to the phase transformation.

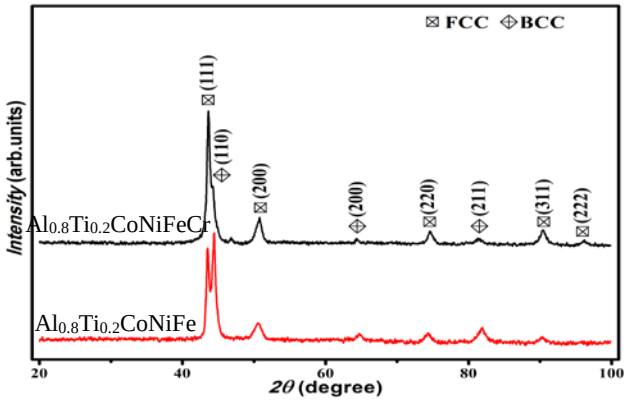

Fig. 3.1.2: XRD patterns of bulk $Al_{0.8}Ti_{0.2}CoNiFeCr$ and $Al_{0.8}Ti_{0.2}CoNiFe$ alloys after SPS

Figure 3.1.3 shows SEM images of bulk $Al_{0.8}Ti_{0.2}CoNiFeCr$ and $Al_{0.8}Ti_{0.2}CoNiFe$ alloys after SPS. Normally, in the AlTiCoNiFeCr HEA, the BCC phase can be easily removed by an Aqua Regia solution. With Cr removal, etched areas increase significantly, consistent with the XRD patterns. The EDS/SEM results show that for the bulk $Al_{0.8}Ti_{0.2}CoNiFeCr$ HEA, point 1 is Co-Fe-Cr rich associated with the FCC phase, whereas point 2 is Al-Ni-Ti rich associated with the BCC phase. With Cr removal, that is, for the bulk $Al_{0.8}Ti_{0.2}CoNiFe$ HEA, point 3 is Co-Fe-Ni rich associated with the FCC phase, whereas point 4 is Al-Ti rich associated with the BCC phase. Note that Ni exhibits almost homogeneous distribution in the FCC and BCC phases.

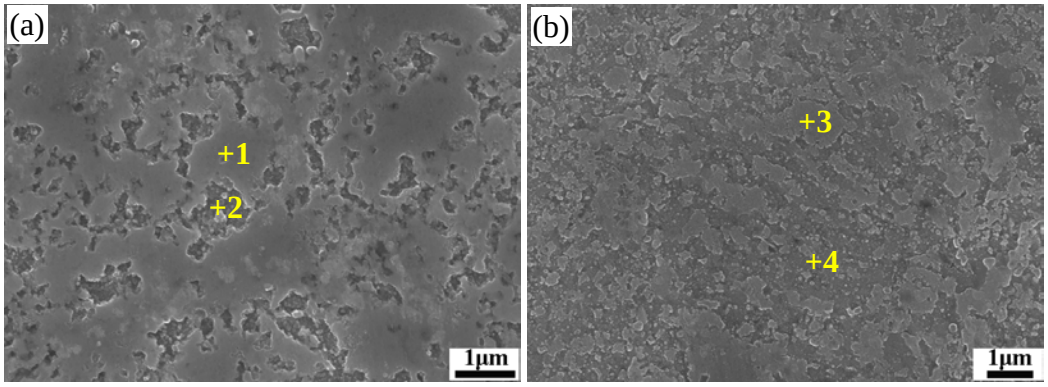

Fig. 3.1.3: SEM micrographs of bulk alloys after sintering. (a) $Al_{0.8}Ti_{0.2}CoNiFeCr$, (b) $Al_{0.8}Ti_{0.2}CoNiFe$.

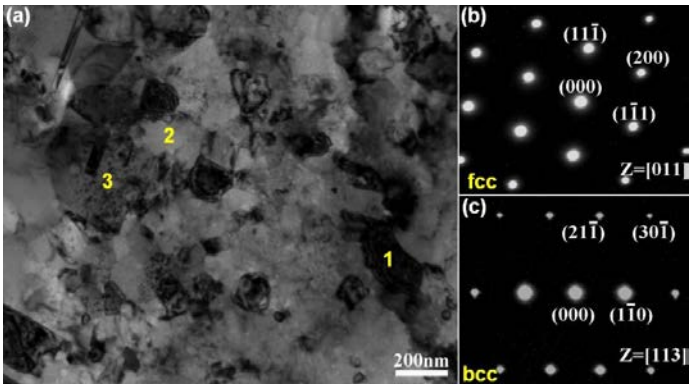

Fig. 3.1.4: TEM micrographs of bulk $Al_{0.8}Ti_{0.2}CoNiFeCr$. (a) Bright field image, (b) SAED pattern of FCC phase along [011] zone axis corresponding to grain1, (c) SAED pattern of BCC phase along [113] zone axis corresponding to grain 2.

Figure 3.1.4 shows the TEM micrographs of bulk $Al_{0.8}Ti_{0.2}CoNiFeCr$ consolidated by SPS. Fig 3.1.4 (a) shows that grain size distribution is from several nanometers to less than 1 μm, confirming a formation of UFG grains. Selected area electron diffraction (SAED) pattern of grain 1 corresponds to that of an FCC structure along [011] zone axis, EDS indicates the FCC phase is Co-Fe-Cr rich. SAED pattern of grain 2 corresponds to that of a BCC structure along [113] zone axis, while EDS indicates that the BCC phase is Ni-Al with some Ti rich. Apparently, twins are observed in grain 3.

Figure 3.1.5 shows the TEM micrographs of bulk $Al_{0.8}Ti_{0.2}CoNiFe$ consolidated by SPS. Bright field image shows that grain size varies from several nanometers to less than 1 μm, confirming a formation of UFG grains. Selected area electron diffraction (SAED) pattern of grain 1 corresponds to that of an FCC structure along [011] zone axis; EDS indicates the FCC phase is Co-Fe with some Ni present. SAED pattern of grain 2 corresponds to that of a BCC structure along [113] zone axis, while EDS indicates that the BCC phase is Ni-Al rich with some Co present. Twins are also observed in this $Al_{0.8}Ti_{0.2}CoNiFe$ HEA, for example, in grain 3.

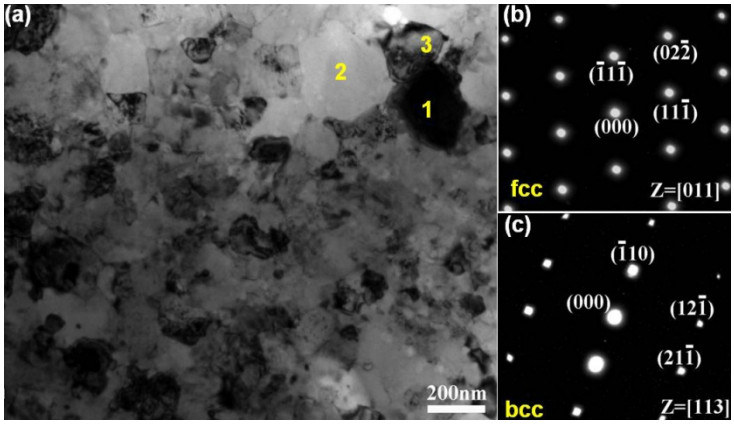

Fig. 3.1.5: TEM micrographs of bulk $Al_{0.8}Ti_{0.2}CoNiFe$. (a) Bright field image, (b) SAED pattern of FCC phase along [011] zone axis corresponding to grain 1, (c) SAED pattern of BCC phase along [113] zone axis corresponding to grain 2.

Influence of Cr removal on mechanical behavior: Figure 3.1.6 shows the engineering stress-strain curves of SPS consolidated $Al_{0.8}Ti_{0.2}CoNiFeCr$ and $Al_{0.8}Ti_{0.2}CoNiFe$ alloys under compression at room temperature. Bulk UFG $Al_{0.8}Ti_{0.2}CoNiFe$ HEA exhibits a higher strength. Compared to bulk UFG $Al_{0.8}Ti_{0.2}CoNiFeCr$ HEA, yield strength, compressive strength and Vickers hardness of bulk UFG $Al_{0.8}Ti_{0.2}CoNiFe$ HEA increase 15.1%, 7.5%, 9.2%, respectively; but strain-to-failure decreases 13.3%. With Cr removal, UFG $Al_{0.8}Ti_{0.2}CoNiFe$ HEA shows higher strength, lower strain, due to the increments of solid-solution strengthening and content of strong BCC phase.

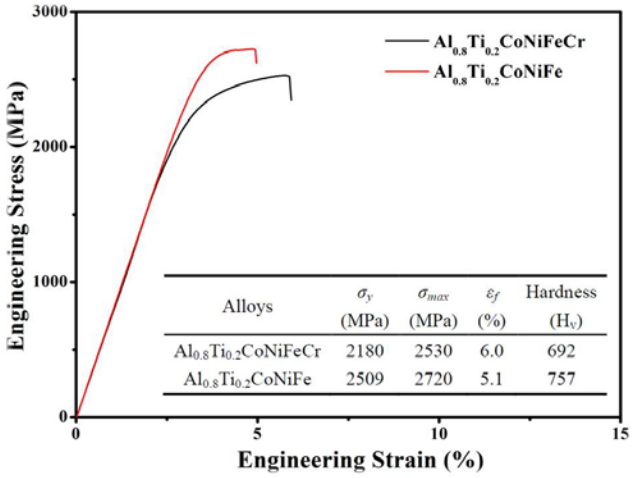

Alloys	σ_y (MPa)	σ_{max} (MPa)	ε_f (%)	Hardness (H_v)
$Al_{0.8}Ti_{0.2}CoNiFeCr$	2180	2530	6.0	692
$Al_{0.8}Ti_{0.2}CoNiFe$	2509	2720	5.1	757

Fig. 3.1.6: Engineering stress-strain curves of consolidated alloys under compression at room temperature.

3.2 Melting and casting of Ingot AlCoCrCuFeNi HEA

The multicomponent AlCoCrCuFeNi alloy (8.5%Al-18.6%Co-16%Cr-20.1%Cu-17.7%Fe-18.6%Ni (wt.%)) was produced in an induction levitation furnace. Repeated melting was carried out at least 4 times to improve the chemical homogeneity of the alloy. The melt was then poured into graphite molds and allowed to solidify. Figure 3.2.1 shows the photo of cast AlCoCrCuFeNi HEA ingots.

Fig. 3.2.1: Melt and cast master alloy of AlCoCrCuFeNi HEA bulk materials.

A typical SEM micrographs of the as-cast HEA are showed in Figure 3.2.2, showing dendritic structure. The microstructure consists of a BCC matrix (dark regions), and FCC phases (lighter regions). The FCC phases located at grain boundaries are larger and brighter than the gray particles located inside the BCC grains (dendrites). Chemical analysis by EDS shows that the inter-dendritic FCC particles have much larger amount of Cu than the intra-dendritic FCC particles. X-ray diffraction analysis of the as-cast sample reveals the presence of a BCC and two FCC phases, as shown in Figure 3.2.3.

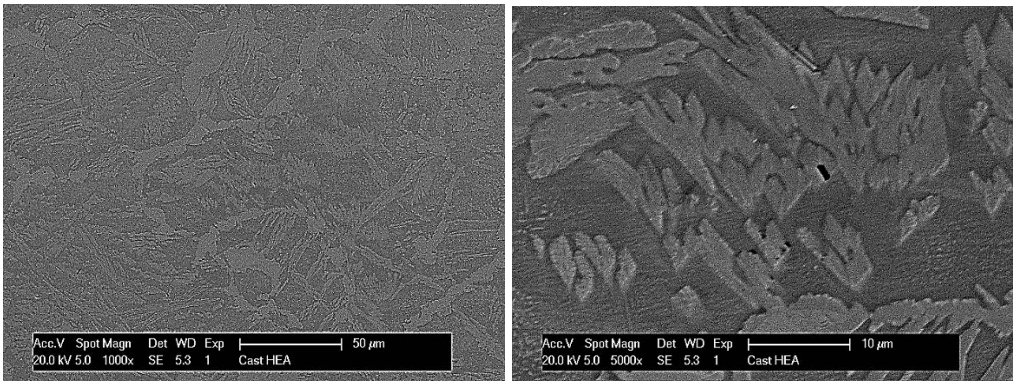

Fig. 3.2.2: SEM micrographs of as-cast AlCoCrCuFeNi HEA ingot.

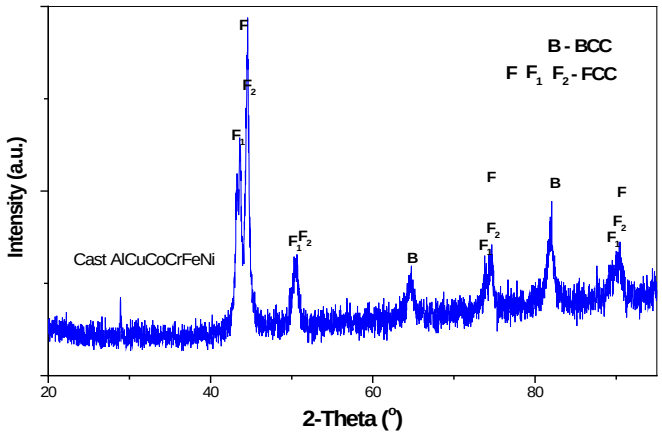

Fig. 3.2.3: XRD pattern of as-cast AlCoCrCuFeNi HEA ingot.

3.3 High Pressure Torsion (HPT) Processing of AlCoCrCuFeNi HEA

The as-cast AlCoCrCuFeNi HEA were sectioned into pieces (Ø10 mm x 1.0 mm) by EDM. With grinding off the surface oxide layer due to EDM, the samples were compressed under HPT at 5 GPa through 2 and 5 turns at room temperature with the rotation speed of 0.5 rpm. Figure 3.3.1 shows the photos of the HPT-processed AlCoCrCuFeNi HEA. The shear strain at edge: $\gamma \approx 78.5$ for 2 turns and $\gamma \approx 196.25$ for 5 turns.

Figure 3.3.2 shows the SEM micrographs of the edge area in HPT-processed AlCoCrCuFeNi HEA for 2 and 5 turns, respectively. The separated/precipitated phases in cast HEA were elongated during HPT. Less phase separation was found in HEA processed with 5 turn of HPT, and microstructure tends to be more uniform with increasing HPT turns. Figure 3.3.3 presents the EDS mapping results of HPT-processed AlCoCrCuFeNi HEA sample (P = 5 GPa, N = 2). The matrix primarily contains Al, Co, Cr, Fe, and Ni. Cu is rich in the lighter grey phases. The fine precipitates inside matrix are rich with Cr, Al, and Ni. Fe and Co are distributed homogeneously in the darker grey phase, but deplete at the interface.

Fig. 3.3.1: Photos of HPT-processed AlCoCrCuFeNi HEA specimens.

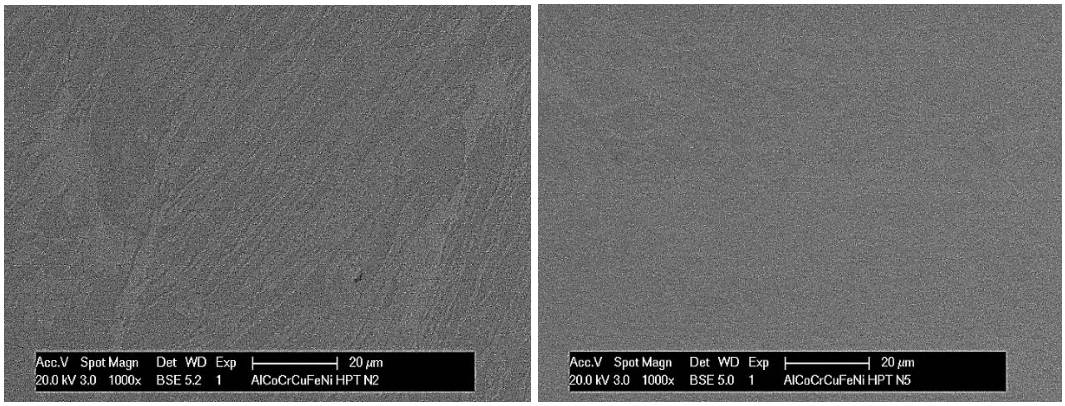

(a) (b)

Fig. 3.3.2: SEM micrographs at the edge of HPT-processed HEA (a) 2-turn and (b) 5-turn sample.

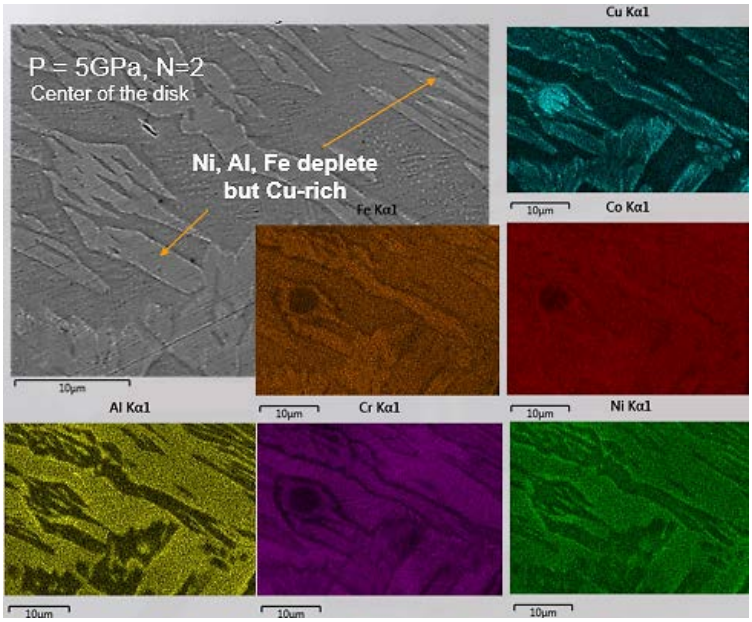

Fig. 3.3.3: EDS mapping of HPT-processed UFG AlCoCrCuFeNi HEA.

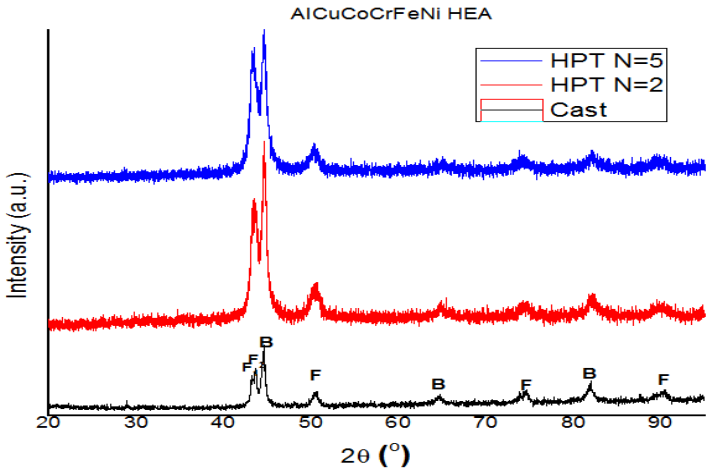

Fig. 3.3.4. XRD patterns of HPT-processed UFG AlCoCrCuFeNi HEA.

Figure 3.3.4 shows the XRD profiles of HPT-processed AlCoCrCuFeNi HEA for 2-turn and 5-turn, respectively. All the XRD curves indicate a mixed FCC and BCC solid solution phases without significant change for both FCC and BCC phases after HPT processing. However, the diffraction peaks broadening was observed for both the FCC and BCC phases after the HPT processing. The diffraction peaks broadening were caused by the lattice strain and the grain size decreasing with the increasing of shear strain. Meanwhile, the intensities of diffraction peaks decrease with the increasing of shear strain. High pressure and shear strain could increase the lattice strain resulting in the significant loss of crystallization perfection and the severe X-ray scattering effect, which is responsible for the decreasing of the peak heights. High pressure and shear strain also resulted in more severe lattice distortion.

The grain size in the as-cast HEA, prior to HPT, was close to about 50 μm. From the BF TEM images in Figure 3.3.5, some clear and wiggled dislocation lines could be seen in the HPT-processed AlCoCrCuFeNi HEA. The grains of the HPT-processed sample transferred from the micrometer-sized coarse grain to strip structure along the direction of the shear strain. The grain size ranges from 600 nm to 1 μm after 2-turn HPT processing. It appears there are still some fraction of coarse grains with rugged and fuzzy boundaries. The dislocation-density increase and dislocation tangling will result in work hardening after HPT. Further increasing the processing strain in HPT might form further refined structure in HEA disks.

Lots of deformation twins were also observed in HPT-processed HEA. Figure 3.3.5 reveals extensive deformation twinning in the AlCoCrCuFeNi HEA deformed by HPT at room temperature. The deformation twins with a thickness from several nanometers to 200 nm were observed. In some areas of the sample, secondary twins could be found. In the initial stage of plastic deformation, primary twins were induced by the shear stress resulting from HPT. Meanwhile, secondary twins and dislocations are constrained by primary twins efficiently. It is obvious that deformation twinning will lead to work hardening. High density of stacking faults, Twin-twin interactions, and de-twining were also observed in HPT-processed HEA. Activated twinning can induce plasticity in HEA.

Vickers microhardness, Hv, against the distance from the disk centers for two HPT conditions (2 and 5 turns) was conducted, and the results are given in Figure 3.3.6 and Table 3.3.1, respectively. The microhardness initially increases with increase HPT Turns. The average microhardness of the HPT-processed samples is 474 HV after 2 revolution, the hardness begins to saturate at the edge. After 5 revolutions the hardness reaches a saturation state with a hardness about 499 HV from the center and extends to the outer edge of the disk. The max hardness reaches 540 HV (5296 MPa), with an equivalent strength (≈ hardness/3) = 1765 MPa. These results agree with the microstructure of the samples processed by HPT, indicating a saturation in grain refinement.

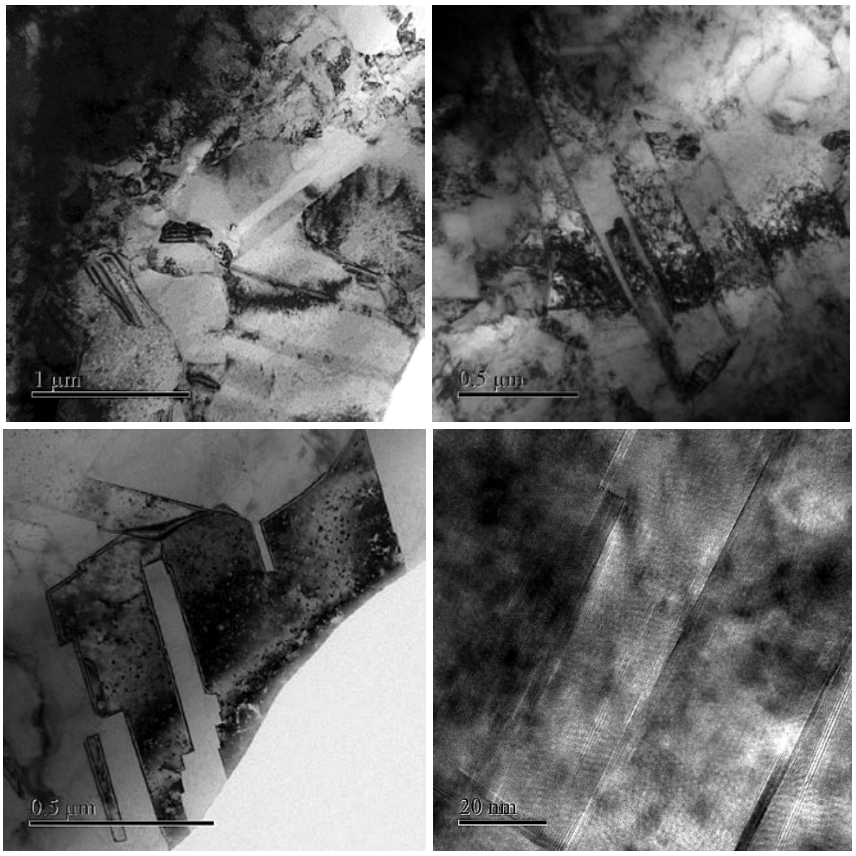

Fig. 3.3.5. TEM micrographs of UFG grains, twins and stack fault structures of 2-turn HPT-processed HEA.

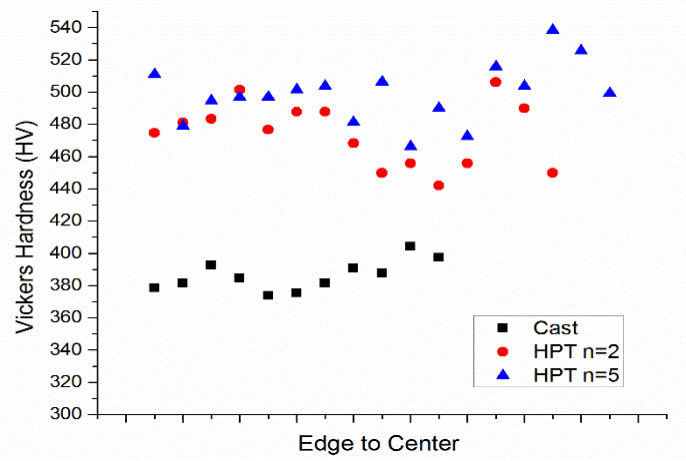

Fig. 3.3.6. Vickers micro-hardness plotted against the distance from the center for HPT-processed HEA samples.

Table 3.3.1. Micro-hardness of HPT-processed AlCoCrCuFeNi HEA

Materials	**Cast**	**HPT (P= 5GPa)**	
		N= 2	**N=5**
Microhardness (HV)	386.1± 9.4	474.0 ± 19.7	498.9 ± 18.4

3.4 Synthesis and processing of UFG AlCoCrCuFeNi HEA

Gas atomization of AlCoCrCuFeNi HEA: Inert gas atomization of the AlCoCrCuFeNi HEA alloy melt was carried out in a confined nozzle atomizer, with melt temperature of 1550^{o}C and gas pressure of 300 psi. The SEM morphology of the AlCoCrCuFeNi HEA alloy powders produced in the atomization is shown in Figure 3.4.1. The surface tension and liquid metal viscosity can influence the morphology of the atomized powders. Spherical morphology was attained in gas atomized AlCoCrCuFeNi HEA powders. The SEM cross-section micrographs of the AlCoCrCuFeNi HEA powder is shown in Figure 3.4.2. There is much less of phase separation in gas atomized HEA powder than that in cast HEA due to high cooling rate in gas atomization depressing phase separation.

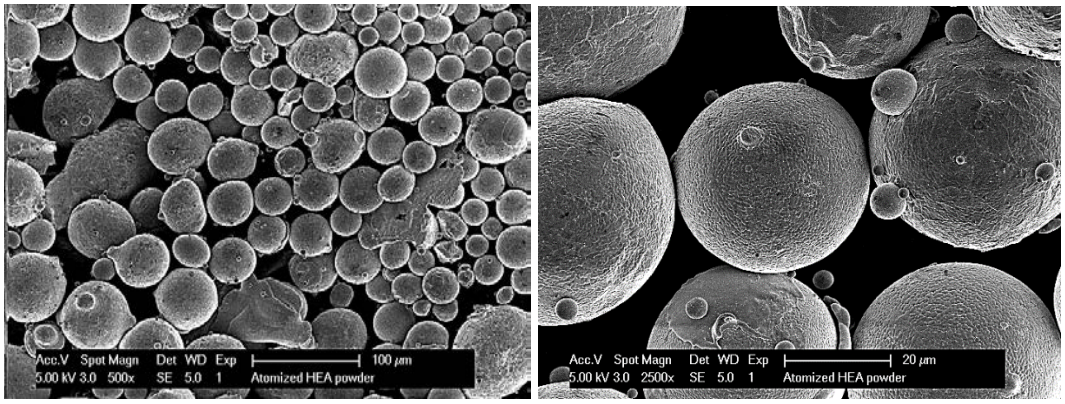

Fig. 3.4.1: SEM morphology of the gas atomized AlCoCrCuFeNi HEA powder.

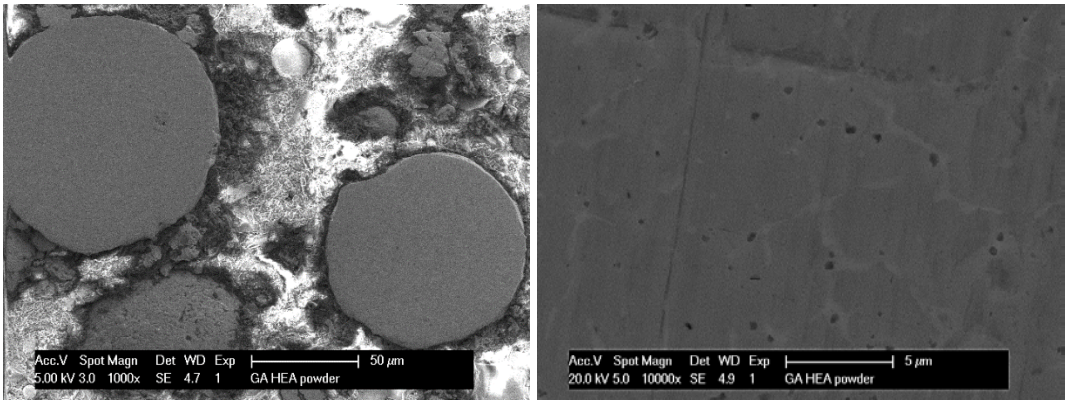

Fig. 3.4.2: SEM micrographs of the cross-section of atomized AlCoCrCuFeNi HEA powder.

Cryomilling of AlCoCrCuFeNi HEA: The cryogenic milling (cryomilling) experiment was performed with liquid N_2 at temperatures -196^{o}C. The atomized AlCoCrCuFeNi HEA powders were cryomilled for 8 hours with a ball-to-powder ratio (BPR) of 20:1 (wt/wt). The typical morphologies of AlCoCrCuFeNi HEA powders evolved after 8 hours cryomilling, are shown in Figures 3.4.3. It is very interesting to observe large amount of shear bands in the cryomilled HEA powder. The morphology of the powder mostly is discoidal, indicating HEAs still have high ductility when deformed at cryogenic temperatures, which might be relate to the shear bands formation, as observed in bulk metallic glasses (BMG).

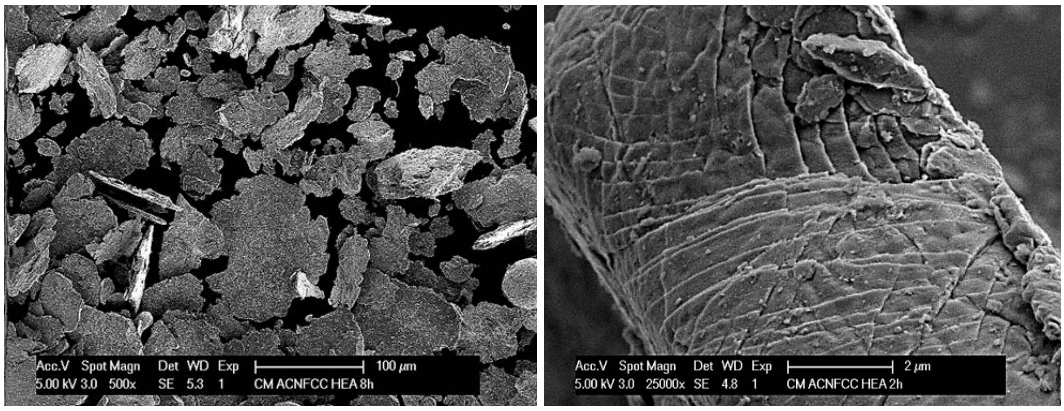

Fig. 3.4.3: SEM micrographs of cryomilled nc AlCoCrCuFeNi HEA Powder.

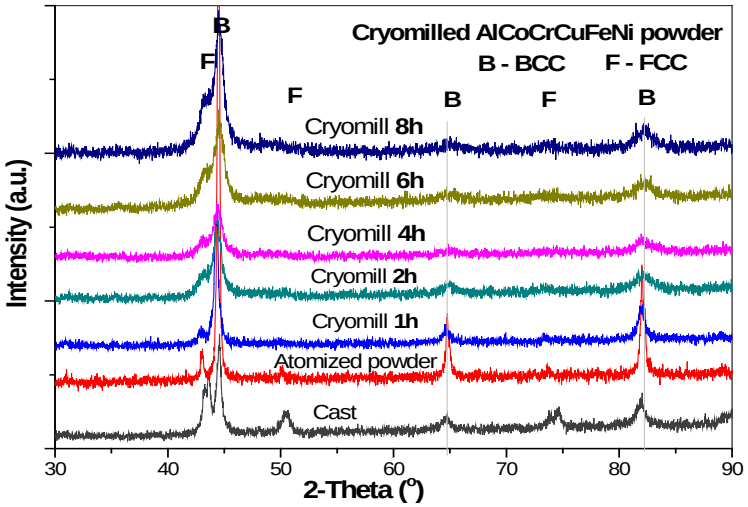

Fig. 3.4.4: XRD patterns of cryomilled AlCoCrCuFeNi HEA powder.

Figure 3.4.4 shows the XRD profiles of cryomilled AlCoCrCuFeNi HEA powder with different milling time, along with those from counterparts under both as-cast and as-atomized conditions. Peak broadening from strong peaks was observed for the cryomilled powders, as compared to those of the gas atomized powder. This peak broadening is attributed to the reduced crystallite size and internal residual micro-strain introduced during cryomilling. It is interesting to note a phase transformation of FCC to BCC found in the cryomilled HEA powder.

SPS consolidation for bulk AlCoCrCuFeNi HEA: Bulk AlCoCrCuFeNi HEA samples were fabricated via SPS from the gas atomized and cryomilled powders, respectively. SPS was performed at different temperatures with 3 minutes of holding time while a heating rate of around 180 ^{o}C/min, and a sintering pressure of 100 MPa, as listed in Table 3.4.1. Figure 3.4.5 shows some SPS-processed HEA disks and then EDM-machined 4x4x5 mm^3 cubic samples for compressive testing.

Fig. 3.4.5: SPS-processed AlCoCrCuFeNi HEA disks and the cubic samples by EDM.

Table 3.4.1. Process conditions for SPS sintering cryomilled powder.

Sample	Powder	Temperature (ºC)	Pressure (MPa)	Time (min)
1	Gas atomized	800	100	3
2		900		
3		1000		
4		1050		
5	Cryomilled	700		
6		800		
7		900		
8		1000		

XRD studies were carried out to identify existing phases as well as variations in grain size in the SPS-processed AlCoCrCuFeNi samples. Figure 3.4.6 shows a comparison in XRD profiles between the SPS-processed bulk samples and the cryomilled HEA powders. The experimental results show that the grain size of HEA increases during SPS process as the XRD peaks of SPS-processed samples are narrower when compared to those of the as-cryomilled powder. It is also interesting to find that there was phase transformation of BCC to FCC during SPS processing.

Figure 3.4.7 presents the DSC results of the gas atomized HEA powder. The endothermic peak, likely related to phase transformation of BCC to FCC, corresponds to the solvus point of the Fe, Cr-rich disordered BCC phase shifted from 638.5°C for the powder to 625.7°C for the cast sample. Two endothermic peaks (1283°C and 1321°C) in the DSC curves for the powder can be attributed to that of Cu–Ni and Fe–Ni FCC solid solutions.

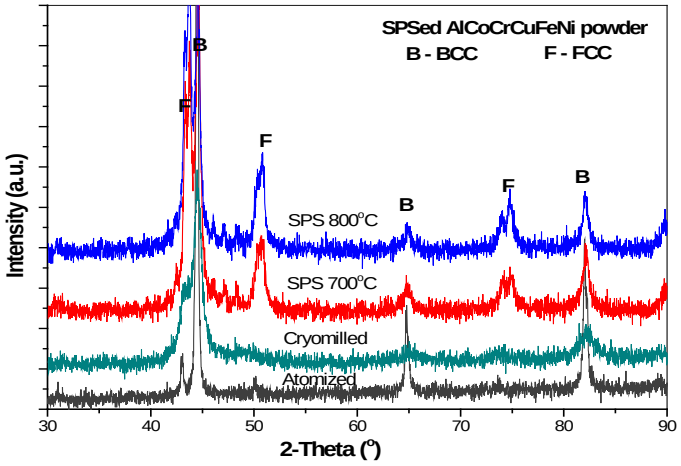

Fig. 3.4.6: XRD patterns of SPS-processed AlCoCrCuFeNi HEA with cryomilled powder.

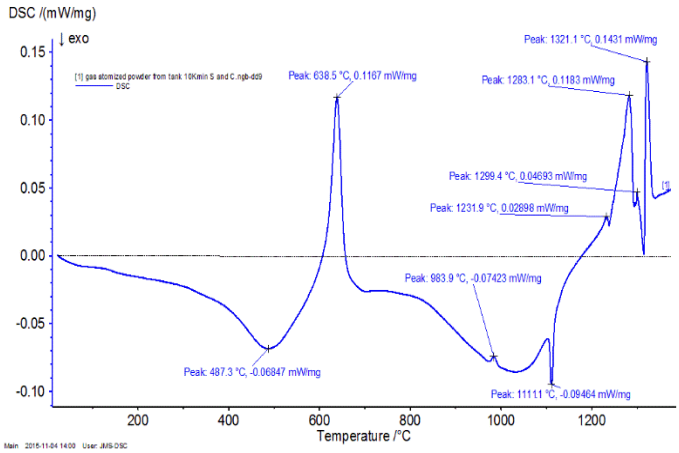

Fig. 3.4.7: DSC result of gas atomized AlCoCrCuFeNi HEA powder.

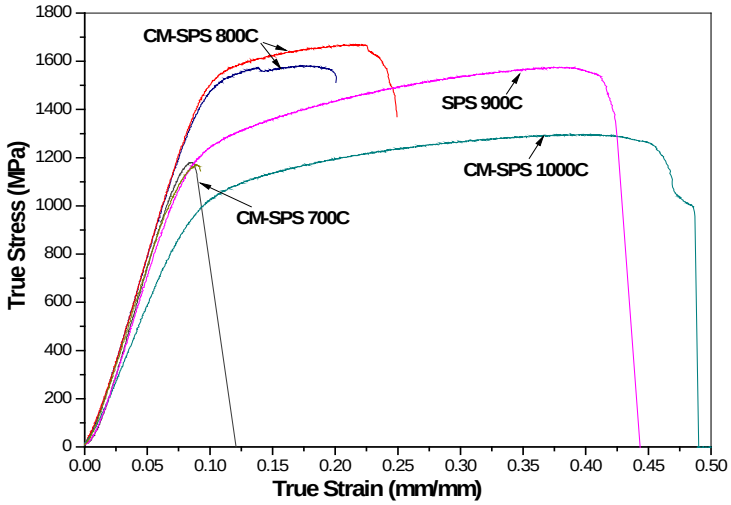

Fig. 3.4.8: Compressive properties of SPS-processed AlCoCrCuFeNi HEA with cryomilled powder.

Table 3.4.2. Mechanical properties of SPS-processed AlCoCrCuFeNi HEA.

SPS conditions	Yield strength	Highest strength	Fracture strain
800ºC	1558 MPa	1680 MPa	0.23
900ºC	1266 MPa	1542 MPa	0.40
1000ºC	1045 MPa	1298 MPa	0.45

Figure 3.4.8 shows the compression behavior of materials with different process parameters, and the corresponding mechanical data are summarized in Table 3.4.2. The highest ultimate strength value for cryomilled and SPS-processed AlCoCrCuFeNi HEA is 1680 MPa (yield strength 1558 MPa) with 23% strain at failure, which is higher than the reported yield strength of as-cast AlCoCrCuFeNi HEA thus far in the literature. The strength values measured for SPS samples decrease with increasing sintering temperature, while the strain at failure increases. Figure 3.4.9 shows the fracture surface of AlCoCrCuFeNi HEA synthesized by SPS at 800ºC. The fine dimples on the fracture surface reflecting the grain size is about 100 to 200 nm. Lamellar structure on the surface inherited from the flat morphologies of initial cryomilled HEA powder.

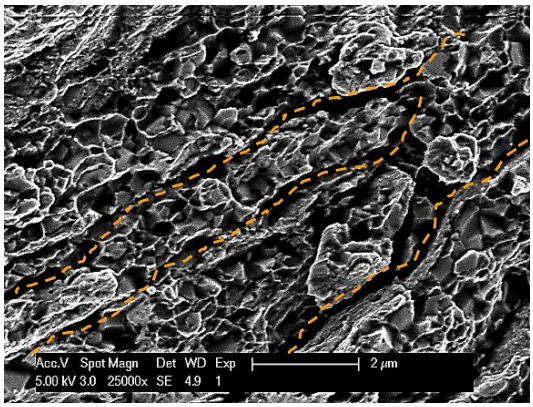

Fig. 3.4.9: Fracture surface of AlCoCrCuFeNi HEA SPS-processed at 800ºC.

3.5 Investigation of microstructure and mechanical behavior of a precipitation-hardened $Fe_{27}Ni_{27}Co_{26}Cu_{10}Ti_{10}$ HEA

The multicomponent $Fe_{27}Ni_{27}Co_{26}Cu_{10}Ti_{10}$ (at.%) alloy was produced in an induction levitation furnace. Repeated melting was carried out at least 4 times to improve the chemical homogeneity of the alloy. The melt was then poured into graphite molds and allowed to solidify.

Figure 3.5.1(a) shows the XRD pattern of the as-cast $Fe_{27}Ni_{27}Co_{26}Cu_{10}Ti_{10}$ HEA, indicating that the as-cast $Fe_{27}Ni_{27}Co_{26}Cu_{10}Ti_{10}$ HEA is composed of a primary fcc phase and a minor unknown phase. The BSE-SEM micrograph in Figure 3.5.1(b) shows that the fcc phase possess equiaxed grain structure, whereas the unknown phase has an elongated morphology.

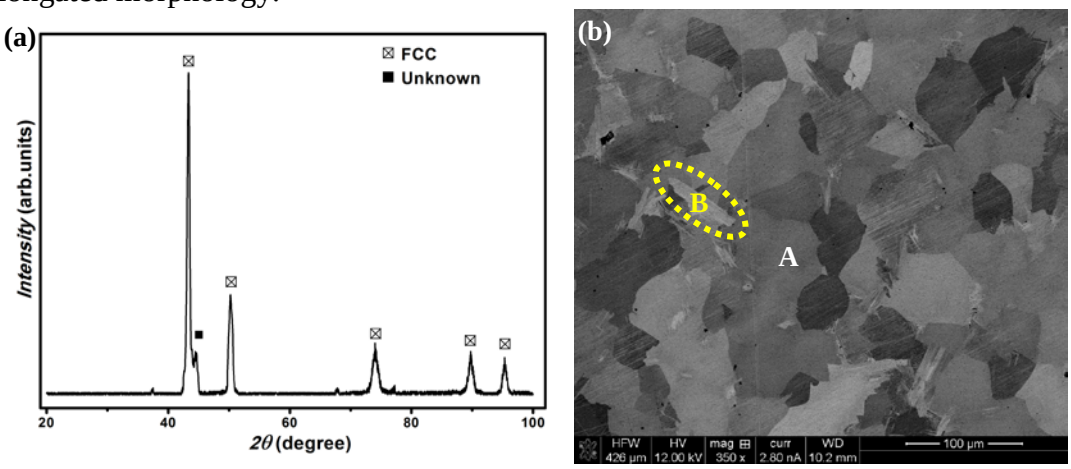

Fig. 3.5.1: (a) XRD, (b) BSE-SEM micrograph of the as-cast $Fe_{27}Ni_{27}Co_{26}Cu_{10}Ti_{10}$.

TEM in Figure 3.5.2 shows that the primary fcc phase (Figure 3.5.2(c)) has a high density of nanoprecipitates, and the corresponding SAED pattern shows an ordered fcc ($L1_2$) structure, suggesting that the matrix and the nanoprecipitates in the fcc phase are coherent. Initial observations show the unknown phase is an ordered phase, but further studies are needed completely identify it.

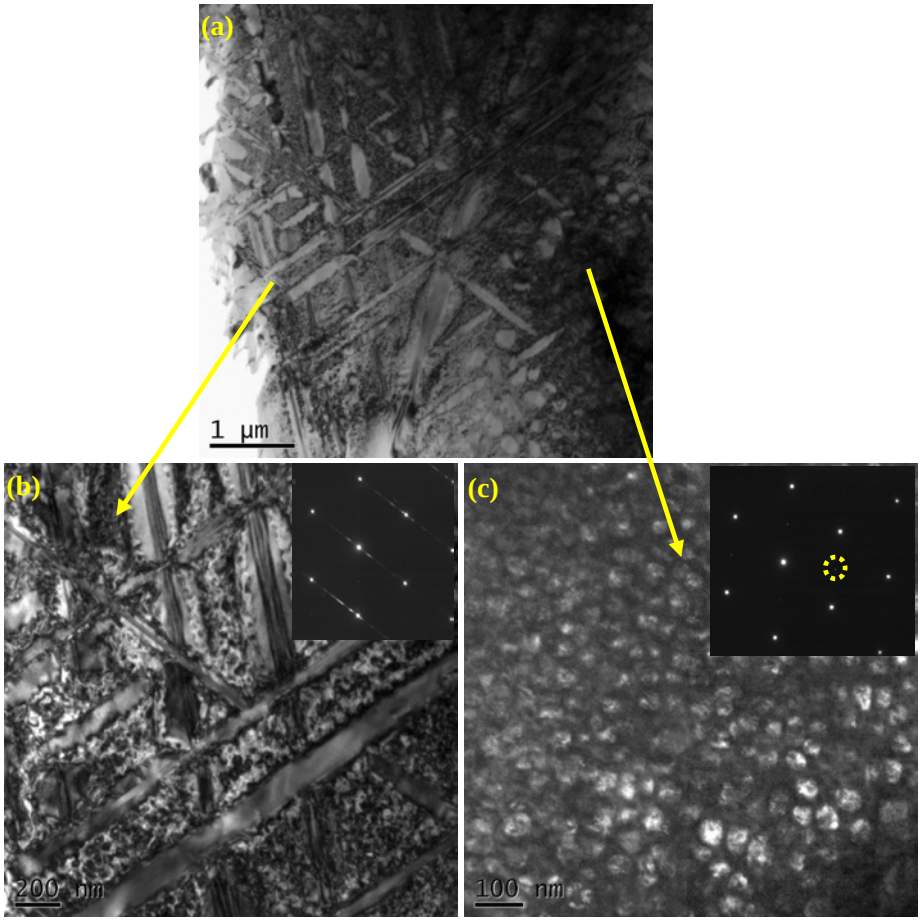

Fig. 3.5.2: TEM of the as-cast $Fe_{27}Ni_{27}Co_{26}Cu_{10}Ti_{10}$.

Figure 3.5.3 shows the stress-strain curves of the as-cast $Fe_{27}Ni_{27}Co_{26}Cu_{10}Ti_{10}$ HEA under compression at room temperature. The true stress-strain curve shows that the as-cast $Fe_{27}Ni_{27}Co_{26}Cu_{10}Ti_{10}$ HEA exhibits yield strength of ~1235 MPa and compressive strength of ~1882 MPa with 33.5% strain at failure.

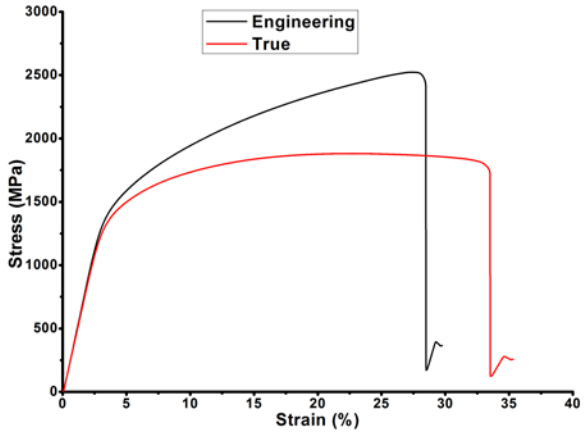

Fig. 3.5.3: Stress-strain curves of the as-cast $Fe_{27}Ni_{27}Co_{26}Cu_{10}Ti_{10}$ HEA.

3.6 Thermal stability and mechanical behavior of a single phased $Fe_{27}Ni_{27}Co_{26}Cu_{10}Mn_{10}$ HEA

The multicomponent $Fe_{27}Ni_{27}Co_{26}Cu_{10}Mn_{10}$ (at.%) alloy was produced in the same manner as the $Fe_{27}Ni_{27}Co_{26}Cu_{10}Ti_{10}$, described in section 3.6. The XRD pattern of the as-cast $Fe_{27}Ni_{27}Co_{26}Cu_{10}Mn_{10}$, Figure 3.6.1(a), confirms the presence of one fcc random solid solution phase. The equiaxed grain structure of this single fcc phase is visible in the BSE-SEM micrograph, Figure 3.6.1(b), in which the contrast is attributed to the unique orientation of each grain.

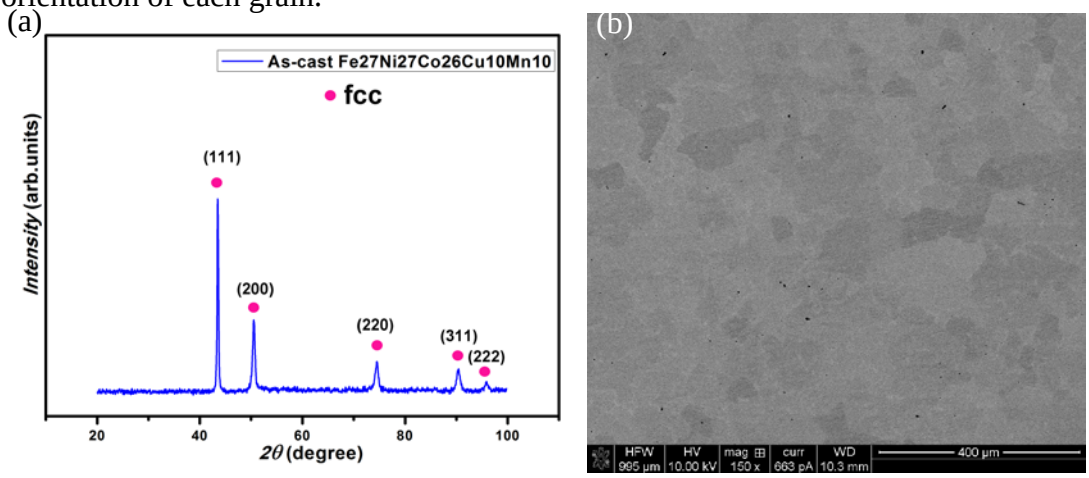

Fig. 3.6.1: (a) XRD, (b) BSE-SEM micrograph of the as-cast $Fe_{27}Ni_{27}Co_{26}Cu_{10}Mn_{10}$.

Thermal stability of the single fcc phase present in the as-cast $Fe_{27}Ni_{27}Co_{26}Cu_{10}Mn_{10}$ was assessed using DSC. Figure 3.6.2 presents the DSC curve of the as-cast $Fe_{27}Ni_{27}Co_{26}Cu_{10}Mn_{10}$, from which no thermodynamic events are observed until the solidus point for the alloy at 1304°C.

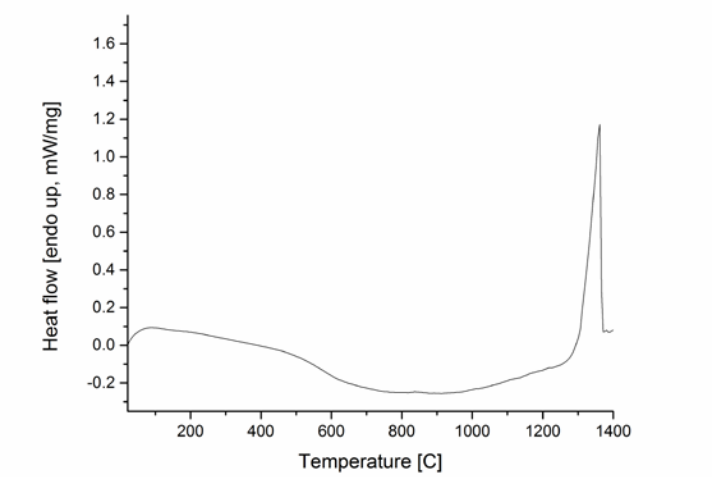

Fig. 3.6.2: DSC result of as-cast $Fe_{27}Ni_{27}Co_{26}Cu_{10}Mn_{10}$.

Figure 3.6.3 shows the stress-strain curves of the as-cast $Fe_{27}Ni_{27}Co_{26}Cu_{10}Mn_{10}$ HEA under compression at room temperature. The true stress-strain curve shows that the as-cast $Fe_{27}Ni_{27}Co_{26}Cu_{10}Mn_{10}$ HEA exhibits a yield strength of roughly 245 MPa. The test was stopped once the sample did not fracture after nearly 85% strain. Further tests of the mechanical behavior of the as-cast $Fe_{27}Ni_{27}Co_{26}Cu_{10}Mn_{10}$ HEA in tension are planned.

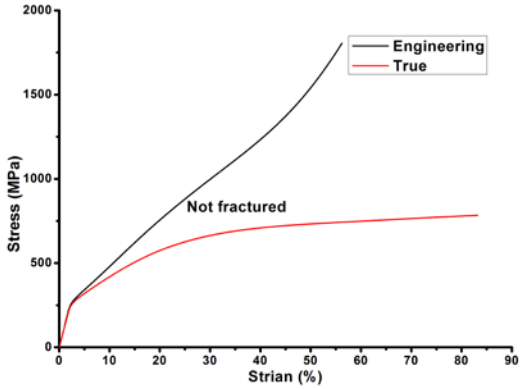

Fig. 3.6.3: Stress-strain curves of the as-cast $Fe_{27}Ni_{27}Co_{26}Cu_{10}Mn_{10}$ HEA.